Direct measurement of $|V_{ts}|$ from $t \to Ws$ decay at FCC-ee

Sofia Giappichini[1], Jan Kieseler[1], Markus Klute[1], Matteo Presilla[1], Aaron Wiedl[1], and Xunwu Zuo[1]

[1]Institute for Experimental Particle Physics (ETP), Karlsruhe Institute of Technology (KIT), Wolfgang-Gaede-Straße 1, D-76131, Karlsruhe, Germany

Contents

1 Introduction

The CKM matrix elements are fundamental parameters of the Standard Model (SM). For $|V_{ts}|$ in particular, the current best determination comes from the $B_s^0 - \bar{B}_s^0$ mixing, which is mediated by box diagrams with top quarks and W bosons. The PDG [1] value is

$$|V_{ts}| = (41.5 \pm 0.9) \times 10^{-3}, \tag{1}$$

which is based on the lattice QCD calculations of the bag parameters and decay constants [2]. The theory uncertainty from lattice QCD is the dominating uncertainty in this measurement, outweighing the experimental uncertainty, from the Δm_s measurement [1], by about 50 times. Meanwhile, the calculation on the loop-induced process assumes no new physics (NP) in the loop and is model-dependent.

A direct and model-agnostic measurement of $|V_{ts}|$, is possible, can be an important cross-check of the lattice QCD results and can be sensitive to NP that is not probed by the indirect measurements. The proposed $t\bar{t}$ operation of FCC-ee at 365 GeV is expected to yield about 2×10^6 $t\bar{t}$ events, in which the decay chain of top quarks can be fully reconstructed and the final state jet flavor can be identified with excellent efficiency. Such dataset presents the opportunity for a direct measurement of $|V_{ts}|$ via the $t \to Ws$ decay for the first time.

This note presents a study of the expected sensitivity for the $|V_{ts}|$ measurement via the $t \to Ws$ decay at FCC-ee. The analysis is based on fast-simulation with standard FCC-ee specifications, explained in Sec. 2. Different jet clustering algorithms are compared, and the jet flavor tagging performance is evaluated, detailed in Sec. 3. The analysis covers 4 event categories: dileptonic $t\bar{t}$ decays, semileptonic $t\bar{t}$ decays where the hadronic W decay is $W \to cs$, semileptonic $t\bar{t}$ decays where the hadronic W decay is $W \to ud$, and fully hadronic $t\bar{t}$ decays[1], described in Sec. 4. The $t \to Ws$ signal sensitivity is evaluated by binned maximum-likelihood fit, combining 4 event categories, and also interpreted for a determination of $|V_{ts}|$, illustrated in Sec 6.

2 Sample generation

This analysis uses samples generated with the standard procedure of the FCC-ee "winter2023" campaign. A complete list of samples is given in Table 1 to 3. The $t\bar{t}$ and Higgs samples are generated with Whizard v.3.0.3 [3, 4], showered with Pythia6 [5], while the WW and ZZ processes are generated with Pythia8 [6]. All samples are simulated with fast simulation of the IDEA detector concept [7] in Delphes v.3.5.1pre05 [8].

Process	Sample name	Raw events	Cross-section (pb)
$t\bar{t}$, $t \to sW(\to \ell\nu)$, $\bar{t}$ inclusive	wzp6_ee_SM_tt_tWsTWb_tlepTall_ecm365	4730233	0.376×10^{-3}
$t\bar{t}$, $t \to sW(\to$ light hadrons), $\bar{t}$ inclusive	wzp6_ee_SM_tt_tWsTWb_tlightTall_ecm365	4564328	0.376×10^{-3}
$t\bar{t}$, $t \to sW(\to$ heavy hadrons), $\bar{t}$ inclusive	wzp6_ee_SM_tt_tWsTWb_theavyTall_ecm365	4978856	0.376×10^{-3}
$t\bar{t}$, t inclusive, $\bar{t} \to \bar{s}W(\to \ell\nu)$	wzp6_ee_SM_tt_tWbTWs_tallTlep_ecm365	4894704	0.376×10^{-3}
$t\bar{t}$, t inclusive, $\bar{t} \to \bar{s}W(\to$ light hadrons)	wzp6_ee_SM_tt_tWbTWs_tallTlight_ecm365	4396175	0.376×10^{-3}
$t\bar{t}$, t inclusive, $\bar{t} \to \bar{s}W(\to$ heavy hadrons)	wzp6_ee_SM_tt_tWbTWs_tallTheavy_ecm365	4813736	0.376×10^{-3}

Table 1: SM $t\bar{t}$ ($\to Ws$) signal processes considered in this analysis. Full CKM mixing is enabled in the sample generation. The "heavy hadrons" in the table refers to final states that includes c-, b-hadrons, while the "light hadrons" means the decay products do not contain c-, b-hadrons. The cross section values are calculated by assuming a total of 2.0×10^6 $t\bar{t}$ events in the 3.0 ab^{-1} data at 365 GeV, and $\mathcal{B}(t \to Ws) = 1.69 \times 10^{-3}$.

[1] Also sometimes referred to as "dihadronic" decays in the following text

Process	Sample name	Raw events	Cross-section (pb)
$t\bar{t}$, dileptonic	wzp6_ee_SM_tt_tlepTlep_noCKMmix_keepPolInfo_ecm365	5330291	0.071
$t\bar{t}$, $t \to$ lep $\bar{t} \to$ had	wzp6_ee_SM_tt_tlepThad_noCKMmix_keepPolInfo_ecm365	5412033	0.146
$t\bar{t}$, $t \to$ had $\bar{t} \to$ lep	wzp6_ee_SM_tt_thadTlep_noCKMmix_keepPolInfo_ecm365	5329449	0.146
$t\bar{t}$, dihadronic	wzp6_ee_SM_tt_thadThad_noCKMmix_keepPolInfo_ecm365	5329622	0.303

Table 2: SM $t\bar{t}$ processes considered as backgrounds in this analysis. CKM mixing is disabled in these samples, therefore they do not contain signal events. The cross section values are calculated by assuming a total of 2.0×10^6 $t\bar{t}$ events in the 3.0 ab^{-1} data at 365 GeV.

Process	Sample name	Raw events	Cross-section (pb)
WW	p8_ee_WW_ecm365	100754213	10.71
ZZ	p8_ee_ZZ_ecm365	61470944	0.643
$Z \to b\bar{b}$	p8_ee_Zbb_ecm365	55932700	4.056
$Z \to c\bar{c}$	p8_ee_Zbb_ecm365	55879156	4.506
$Z \to s\bar{s}$	p8_ee_Zbb_ecm365	55848129	4.084
$Z \to u\bar{u}/d\bar{d}$	p8_ee_Zqq_ecm365	55742194	8.679
$Z \to \tau\bar{\tau}$	wzp6_ee_tautau_ecm365	12800000	2.017
bbH	wzp6_ee_bbH_ecm365	1100000	0.01838
ccH	wzp6_ee_ccH_ecm365	900000	0.01443
ssH	wzp6_ee_ssH_ecm365	900000	0.01853
qqH	wzp6_ee_qqH_ecm365	2400000	0.03299
$\tau\tau H$	wzp6_ee_tautauH_ecm365	1100000	0.00417
$\mu\mu H$	wzp6_ee_mumuH_ecm365	1200000	0.00418
eeH	wzp6_ee_eeH_ecm365	1000000	0.00739
$\nu\nu H$	wzp6_ee_nunuH_ecm365	2200000	0.05394
WWZ	wzp6_ee_WWZ_Zbb_ecm365	12800000	0.00202

Table 3: Other SM processes considered as backgrounds in this analysis. The cross sections are taken directly from the generator.

3 Jet definition and flavor tagging

Jet reconstruction and jet flavor identification is the core of this work. The efficiency for identifying jets stemming from an s quark is a crucial component in this analysis. In addition, the expected uncertainty for calibrating such s quark tagger directly translates to the uncertainty in the measurement of $|V_{ts}|$. The corresponding studies are described in Sec. 3.1 and 3.2.

3.1 Jet clustering

Two clustering algorithms are tested for this analysis: the exclusive jet clustering (*ee kT*, or Durham, algorithm) and the inclusive jet clustering (*ee* generalised *kT* algorithm), both provided by the FastJet package [9].

Exclusive jets: the distance between sub-jets is defined as

$$d_{ij} = 2\min(E_i^2, E_j^2)(1 - \cos\theta_{ij}) \tag{2}$$

Inclusive jets: the distance between sub-jets is defined as

$$d_{ij} = \min(E_i^{2p}, E_j^{2p})\frac{1 - \cos\theta_{ij}}{1 - \cos R} \tag{3}$$

Subjets are merged until no d_{ij} is smaller than $d_{iB} = E_i^{2p}$. In these equations, i and j are the indices for sub-jets, p and R are general parameters in the distance calculation, and θ_{ij} is the open angle between the sub-jets.

In this study, the *ee* kT clustering is considered with $N = 2, 4, 6$ cases, hereafter referred to as kt2, kt4, and kt6 jets. The *ee* gen-kT clustering is tested with $p = -1$, $R = 0.5, 0.8, 1.0$ cases, hereafter referred to as R5, R8, and R10 jets. The jet clustering considers all reconstructed particles in the event except muons and electrons with energy above 10 GeV, which are masked from jet clustering.

The jet energy and jet mass with different jet definitions are compared in Fig. 1. All inclusive jet definitions feature a peak at very low energy, representing isolated clusters of soft activities. A minimum energy cut is therefore necessary for inclusive jets. A long tail on the high mass side of jet mass distribution is present, particularly for large radius jets, which depicts hadronization products originating from different quarks clustered into a single jet. A cut of jet mass is posed to remove those edge cases while retaining high efficiency for regular jets. Hereafter, a selection of $m_j < 50$ GeV and $E_j > 15$ GeV is applied to all inclusive jets.

Between dileptonic events (upper row), where 2 hard jets are expected, and semileptonic events (lower row), where 4 hard jets are expected, the inclusive jets clustering shows a consistent shape in jet mass and energy profiles. The exclusive jet clustering, by definition, only works when the number of true jets matches the required number of clusters. As expected, the kt2 jet clustering shows very different behavior with semileptonic events.

3.2 Flavor tagging

The official flavor tagging algorithm at FCC-ee [10] is based on ParticleNet [11]. The training is performed on 240 GeV $e^+e^- \to ZH$, $Z \to \nu\nu, H \to gg$, qq, or $\tau\tau$ events, where $q = u, d, s, c, b$, with *ee* kT jets. The tagger score is normalized such that the sum of all labels equals 1. In this analysis, we apply this tagger to all selected jets and decide the jet flavor by requiring the corresponding label score > 0.5. The events used in this analysis are at a different collision energy from the events used for the training, and the jets are built with a different clustering algorithm. The flavor tagging performance needs to be validated. Appendix B shows the evaluation of tagger performance.

4 Event selection

The $t\bar{t}$ events decay to many distinct final states, and the corresponding background composition can be very different. All events are required to contain one b-tagged jet (b-score > 0.5) and at least one s-tagged jet (s-score > 0.5). Events are further divided into 10 orthogonal categories, each targeting a distinct final state[2]:

- **dilep_0tau**: dileptonic category containing two light leptons (e or μ), which are oppositely charged.

[2] As described in App. A, an issue in background samples produced specifically for this analysis may affect the modeling of events with τ decays. To be safe, this document describes the analysis in all event categories, but only categories without τ leptons are considered for the final result.

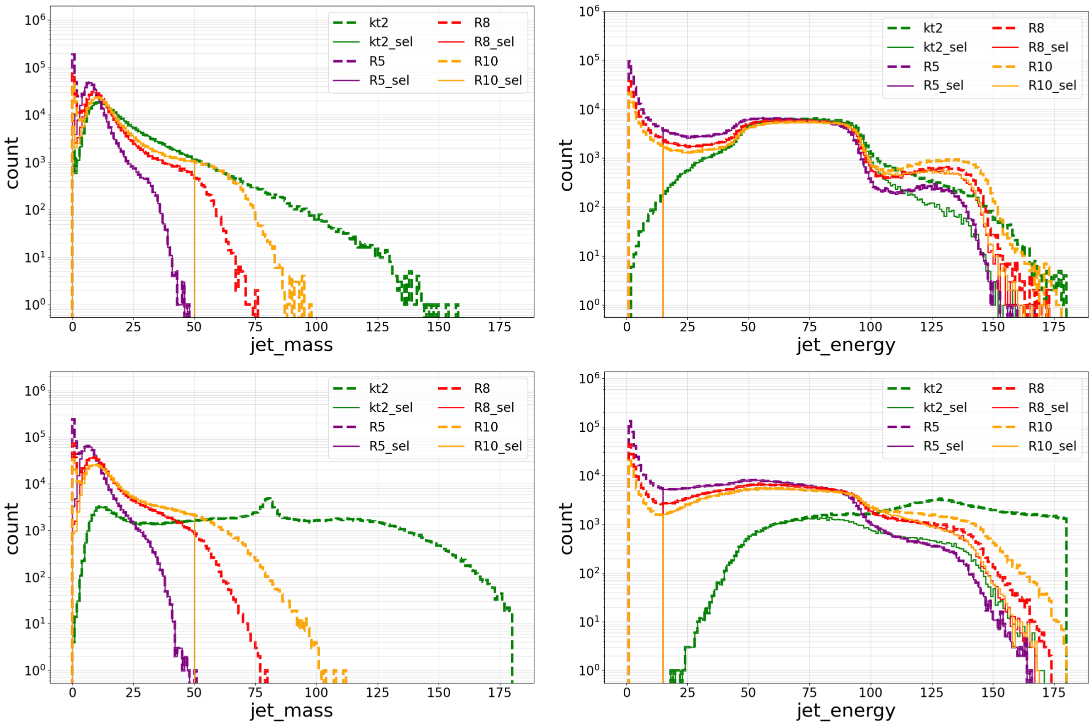

Figure 1: Jet mass and energy distributions, comparing jet definition of kt2, R5, R8, and R10. The upper row shows the jet reconstructed in dileptonic $t\bar{t}(t \to Ws)$ events, and the lower row shows semileptonic $t\bar{t}(t \to Ws)$ events. The dash lines are jet properties prior to any selection, while the solid lines are after the selection of $m_j < 50$ GeV and $E_j > 15$ GeV.

- **dilep_1tau**: dileptonic category containing one light lepton (e or μ) and one hadronic τ decay (τ-score > 0.5).
- **dilep_2tau**: dileptonic category containing two hadronic τ decay (τ-score > 0.5).
- **semilep_0tau_ud**: semileptonic category containing one light lepton (e or μ) and one u- and d-tagged jet pair (u-, d-score > 0.5).
- **semilep_0tau_cs**: semileptonic category containing one light lepton (e or μ) and one c- and s-tagged jet pair (c-, s-score > 0.5).
- **semilep_1tau_ud**: semileptonic category containing one hadronic τ decay and one u- and d-tagged jet pair.
- **semilep_1tau_cs**: semileptonic category containing one hadronic τ decay and one c- and s-tagged jet pair.
- **dihad_ud_only**: fully hadronic category containing no lepton and two u- and d-tagged jet pairs.
- **dihad_udcs**: fully hadronic category containing no lepton, one u- and d-tagged jet pairs, and one c- and s-tagged jet pair.
- **dihad_cs_only**: fully hadronic category containing no lepton and two c- and s-tagged jet pairs.

Electrons and muons are selected with energy $E_\ell > 20$ GeV, and relative isolation in a cone of 0.5 $I_{R<0.5} < 0.25$. Jets are defined with the inclusive R5 clustering, masking electrons and muons with energy above 10 GeV, with additional selections of $m_j < 50$ GeV and $E_j > 15$ GeV. Both hadronic τ decays are identified from jets with the requirements of $m_j < 50$ GeV and τ-score > 0.5.

These basic category selections are very effective in selecting the target signal decays are reducing background processes. The signal efficiency is summarized in Fig. 2. All event categories achieve the purpose of selecting targeted decay modes. Table 4 summarizes the event yield of all processes. Good signal purities are achieved in all categories.

Categories	dilep_0tau	dilep_1tau	semilep_0tau_ud	semilep_0tau_cs	semilep_1tau_ud	semilep_1tau_cs	dihad_ud_only	dihad_udcs	dihad_cs_only
sig modes									
dilep_0tau	109.535	5.879	0.570	0.003	0.018	0.000	0.000	0.000	0.000
dilep_1tau	10.561	59.169	0.583	0.024	0.136	0.001	0.000	0.000	0.000
dilep_2tau	0.234	3.699	0.020	0.002	0.112	0.004	0.000	0.000	0.000
semilep_0tau_ud	0.000	0.097	247.336	1.269	6.613	0.028	2.289	0.045	0.000
semilep_0tau_cs	0.000	0.043	32.103	78.878	0.825	1.960	0.250	0.674	0.003
semilep_1tau_ud	0.000	0.010	16.048	0.084	57.744	0.315	1.840	0.420	0.002
semilep_1tau_cs	0.000	0.003	2.017	5.023	7.349	18.715	0.205	0.767	0.030
dihad_ud_only	0.000	0.000	0.001	0.000	0.107	0.000	150.641	4.266	0.005
dihad_udcs	0.000	0.000	0.001	0.000	0.060	0.024	40.614	105.374	0.458
dihad_cs_only	0.000	0.000	0.000	0.000	0.011	0.008	2.672	18.875	10.944
bkg modes									
dilep	269.454	160.914	21.037	0.438	0.737	0.053	0.058	0.000	0.000
semilep_ud	1.065	17.042	1827.448	119.534	541.209	38.093	95.711	15.923	0.164
semilep_cs	12.403	197.735	1058.422	544.304	327.451	172.836	27.746	35.177	0.601
dihad	0.000	0.000	21.718	6.361	91.438	30.054	3947.856	3287.219	236.189
Z	8.404	0.872	10.795	1.767	24.512	3.122	276.710	75.150	0.923
WW	8.615	176.456	151.567	6.701	117.744	27.761	613.926	421.197	6.382
ZZ	33.159	22.869	13.521	2.478	16.783	3.796	65.346	47.966	0.596
higgs	22.377	14.851	48.826	5.516	19.929	3.835	156.437	138.137	2.040
WWZ	0.671	0.106	5.736	0.061	0.681	0.000	2.482	0.459	0.005

Table 4: Yield table in all categories, except the dilep_2tau category, after basic event selection.

5 DNN training

After the category selection, a deep neural network (DNN) is trained in each category to optimize the separation between signals and backgrounds. The DNN take the full kinematic information of the selected objects, summarized below:

- **lepton (e/μ) variables**: η and energy of each lepton
- **τ variables**: 4-momentum and τ-score of τ each candidate
- **jet variables**: 4-momentum and flavor tagging score of each jet
- **missing energy variables**: 4-momentum of missing energy

Each DNN is a binary classifier containing 3 hidden layers. The number of nodes of the hidden layers are $\{2 \times n_{\text{input}},\ 4 \times n_{\text{input}},\ 8\}$. For $t\bar{t} \to WbWs$ signal and $t\bar{t} \to WbWb$ background samples, statistically independent events are used for training and analysis. For other background samples, as the total number of events after category selection is limited, the same set of events is used for training and analysis. In the training, a 70%:30% event splitting is made for the training and testing datasets to make sure the DNNs are not overtrained. Figure 3 shows the DNN score of each category, except the "dilep_2tau" category. The ROC curves and overtraining plots are detailed in App. C.

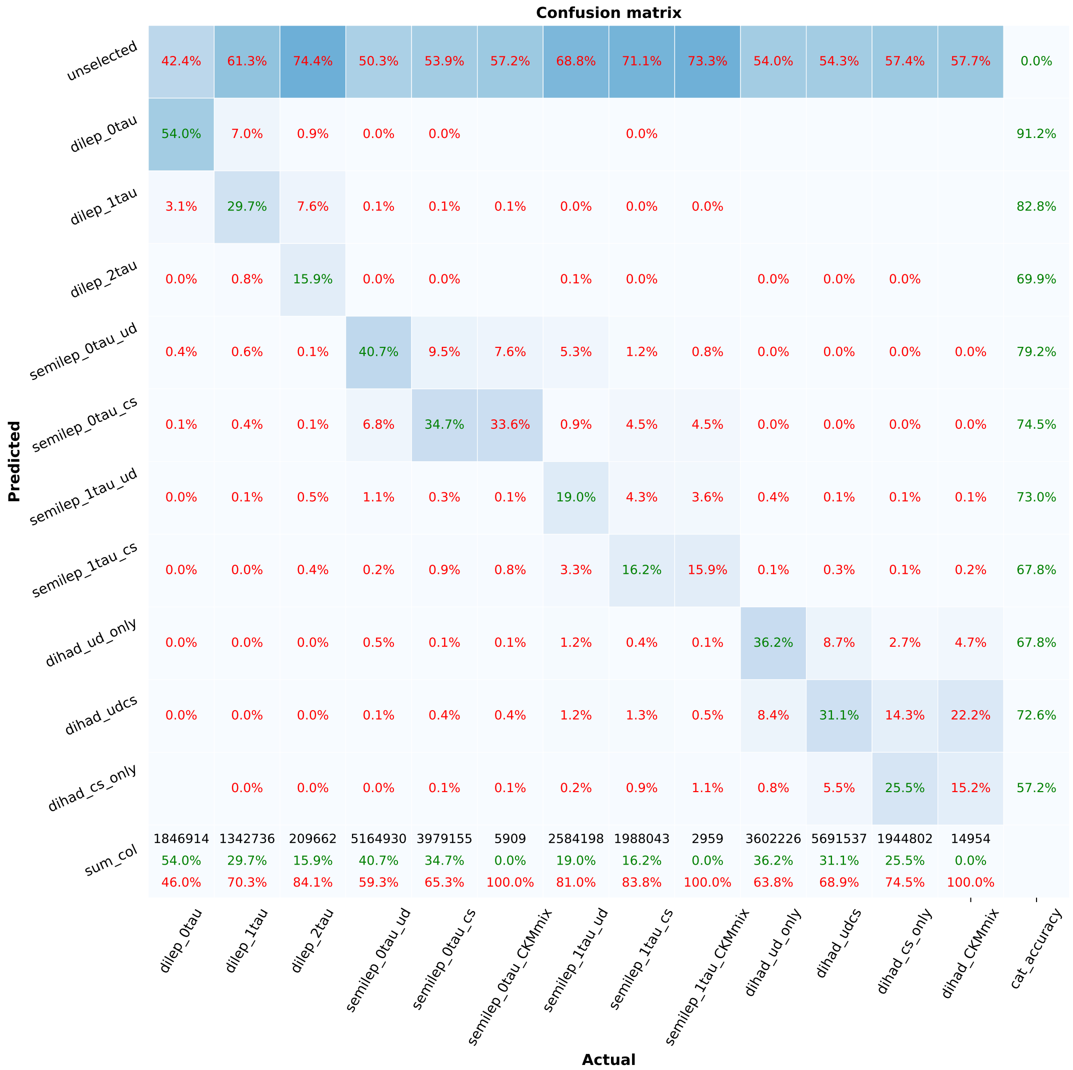

Figure 2: Confusion matrix for signal selection efficiency. The label in each column shows the true decay mode, and the label in each row shows the event category based on reconstructed objects. The number of events shown in the last row is the total number of events for each true decay, before any selection, and the percentage in each cell is the fraction of events selected for the corresponding category. The last column is calculated as the ratio between the events in the diagonal cell and the total events in its row, representing the accuracy of signal selection.

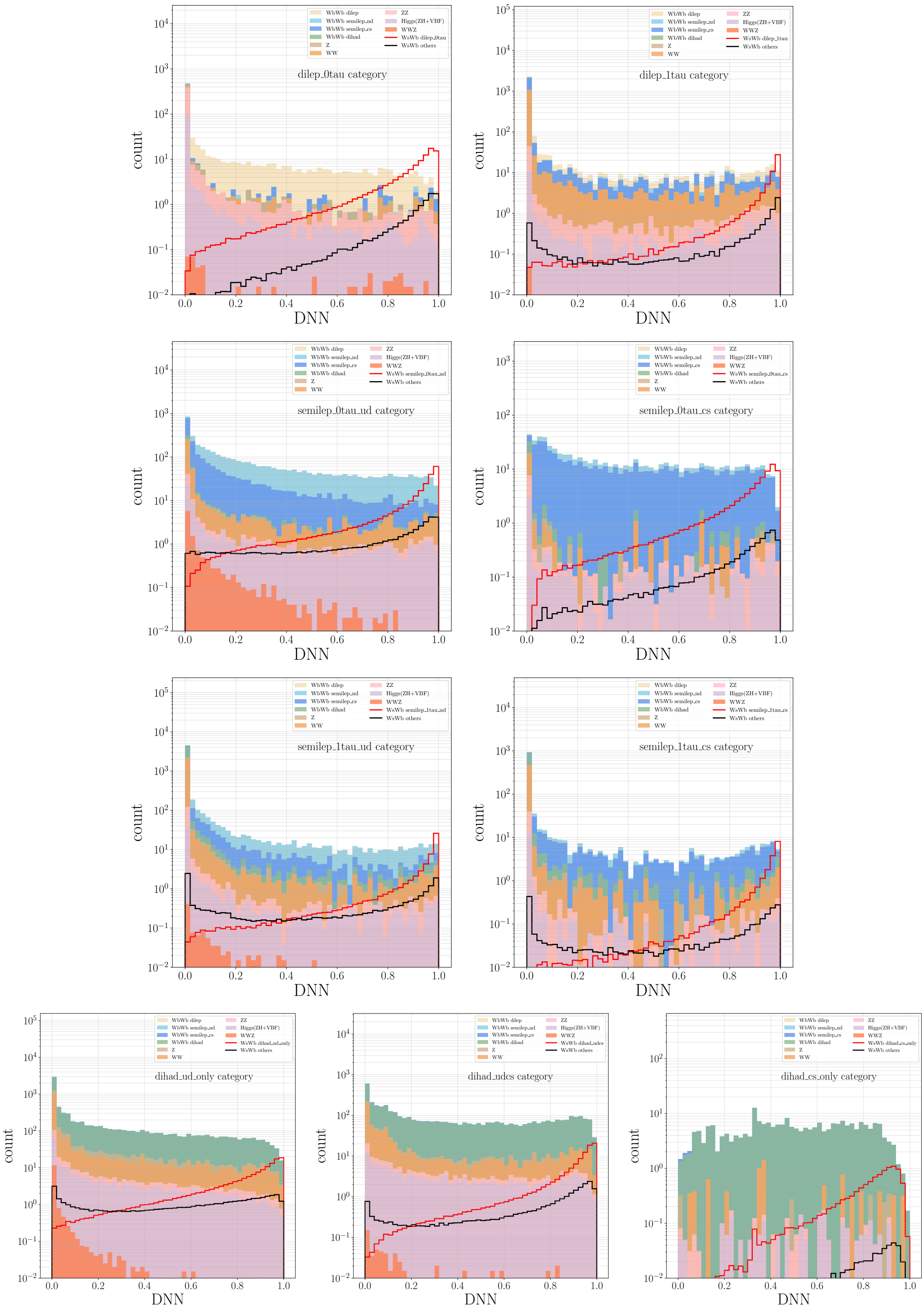

Figure 3: DNN score, in reading order, in dilep_0tau, dilep_1tau, semilep_0tau_ud, semilep_0tau_cs, semilep_1tau_ud, semilep_1tau_cs, dihad_ud_only, dihad_udcs, and dihad_cs_only categories.

6 Results

In all categories, the DNN score distribution with 50 bins, as shown in Fig. 3 is used for signal extraction. The binned maximum-likelihood fit is performed with the CMS Combine tool [12]. This analysis is mostly limited by statistical uncertainty. therefore the most important systematic uncertainties come from the background yields. A background normalization uncertainty is set on each group of backgrounds: Z, WW, ZZ, Higgs, WWZ, and 4 types of $t\bar{t}$ backgrounds (dileptonic, semileptonic_ud, semileptonic_cs, and fully hadronic). Several assumptions on the background uncertainty are tested: all backgrounds freely floating, and all backgrounds constrained to either 20%, 5%, 2%, or 1% of their nominal yields. To be free from the issue in background simulation with τ described in App. A, we consider only categories not involving τ leptons for the combination. The fit results are summarized in Table 5. Fit results including τ categories are also provided in App. D for comparison, but are not considered as the nominal result.

Fit config	Free bkg	bkg ±20%	bkg ±5%	bkg ±2%	bkg ±1%
category					
dilep_0tau	14.5%	12.4%	12.0%	11.9%	11.8%
semilep_0tau_ud	13.2%	10.8%	10.2%	9.9%	9.7%
semilep_0tau_cs	30.3%	18.9%	18.3%	17.8%	17.7%
dihad_ud_only	25.4%	20.2%	19.8%	19.1%	18.6%
dihad_udcs	32.4%	26.0%	25.6%	24.7%	24.1%
dihad_cs_only	108%	83.1%	78.4%	76.5%	76.2%
combined	6.8%	6.6%	6.5%	6.4%	6.3%

Table 5: Relative uncertainty on $\mathcal{B}(t \to Ws)$ measurement combining all categories without τ leptons. Scenarios for background normalization uncertainty are considered: totally free normalization, 20%, 5%, 2%, and 1% variation from nominal yields.

The signal precision is stable against large background uncertainties and gradually improves as the backgrounds become more constrained. As all relevant background processes are expected to be well-measured at FCC-ee. We consider 1% background uncertainty to be a reasonable yet conservative value for the background systematic uncertainty. In this scenario, the combined precision for the $\mathcal{B}(t \to Ws)$ measurement is 6.3%.

7 Conclusion and outlook

As the Branching ratio of $t \to Ws$ decay is directly determined by the $|V_{ts}|$ element.

$$\mathcal{B}(t \to Ws) = |V_{ts}|^2/\Sigma_{d_i}|V_{td_i}|^2, \quad d_i = d, s, b \tag{4}$$

The measurement on $\mathcal{B}(t \to Ws)$ with relative precision $\sigma_{\mathcal{B}(t\to Ws)} = 6.3\%$ can be converted to a measurement on $|V_{ts}|$ with relative precision $\sigma_{|V_{ts}|} = 3.1\%$. This precision is comparable to the current PDG precision [1], which is about 2.2% and mostly limited by theory uncertainty. This measurement at FCC-ee can be the first opportunity for a high-precision direct $|V_{ts}|$ measurement and an important input to the interpretation of flavor measurements involving $b \to s, b \to d$, or $s \to d$ transitions.

For further studies, background samples will be regenerated so that the τ decays can be well modeled and included in the combined results. This analysis can also be extended to a simultaneous measurement of $\mathcal{B}(t \to Ws)$ and $\mathcal{B}(t \to Wb)$ for broader physics interpretations. To measure $\mathcal{B}(t \to Wb)$ at a desirable precision, the systematic uncertainties on the total $t\bar{t}$ cross section and the flavor tagging efficiency are crucial and will be the focus of the future aspects of this work.

A Issue with τ leptons in background simulation

In the $t\bar{t}$ background samples produced specifically for this analysis, only negatively charged τ leptons are generated, while all events (phasespace) involving positively charged τ leptons are not produced. This issue does not affect signal samples.

As a temporary fix, the cross section weighing for events without τ leptons has been corrected accordingly in this analysis. In particular, event weights for backgrounds including τ decays are multiplied by a factor of 2 to compensate for the missing τ^+ components. This fix does not correct for the missing background events in the dilep_2tau category, since no $t\bar{t}$ backgrounds with a $\tau^+\tau^-$ pair is generated. After this temporary fix, categories not involving τ leptons are correctly modeled. Categories with one τ leptons are correct in terms of cross section, but may be subject to high order mismodeling due to the potential difference between τ^+ and τ^- in clustering and tagging performance. Category with two τ leptons (dilep_2tau) is not corrected.

For a proper fix, background samples are regenerated with correct configurations. The sample generation will not finish by the freezing of this document, but will be used for further updates.

B Flavor tagging performance

As the jets in this analysis feature a different momentum range and potentially a different clustering algorithm from the jets used for the training, the tagging performance can deviate from the performance presented in the training data. This section shows the tagging performance evaluated with $t\bar{t}$ events at 365 GeV compared to the reference performance in Ref [10]. Ref [10] presents a training with 5 class labels, $g, u/d, s, c, b$, while the actual tagger used in this analysis is an updated training with the same network architecture containing 7 class labels, g, u, d, s, c, b, τ. The performance shown below are based on the old 5-label training, but the conclusion holds for the new training as well.

It is evaluated for each jet definition. The official s-tagging performance is shown in the left plot of Fig. 4 as a reference. The s-tagging performance evaluated with R5 jets is shown in the right plot of Fig. 4. The s-tagging performance evaluated with exclusive jet clustering is shown in Fig. 5.

The s vs b performance is similar among all jet definitions but worse than the reference performance. This is not unexpected, as there are intrinsic kinematic differences between $t\bar{t}$ events at 365 GeV and ZH events at 240 GeV. The performance on exclusive jets is slightly worse than that on R5 jets. This is likely because the jet geometry of exclusive jets is more different from the inclusive jets used in training.

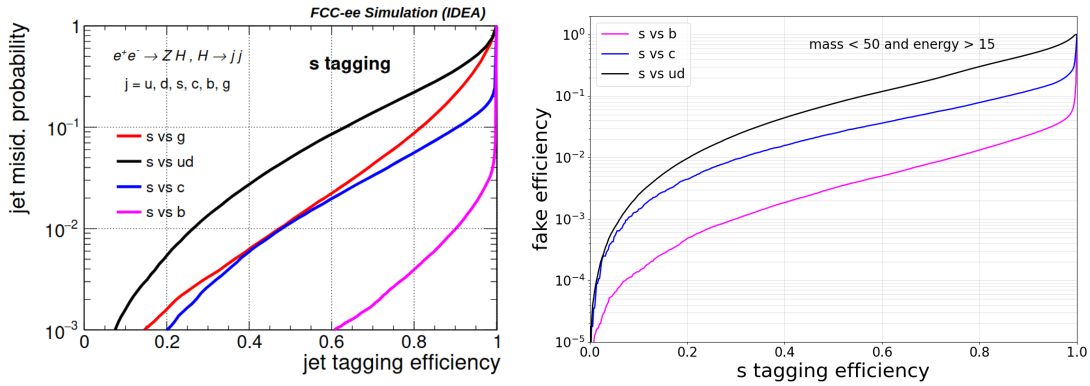

Figure 4: Left: official FCC-ee s-tagging performance, taken from [10]. Right: s-tagging performance of the official tagger evaluated on semileptonic $t\bar{t}(t \to Ws)$ events with R5 jets.

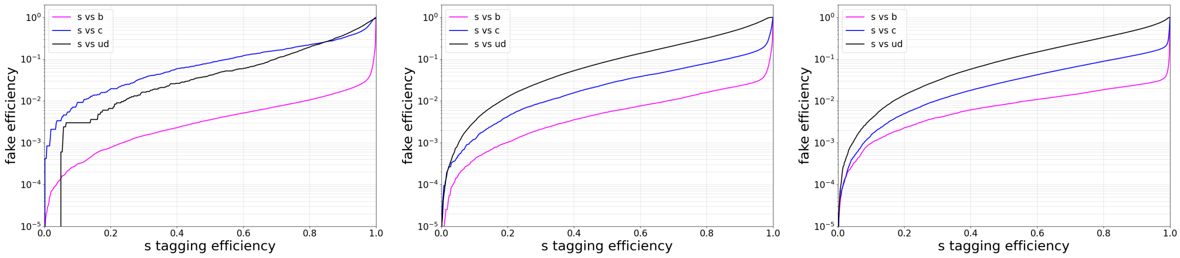

Figure 5: Performance of the official FCC-ee s-tagger evaluated with, from left to right, kt2 jet from dileptonic, kt4 from semileptonic, and kt6 jets from fully hadronic $t\bar{t}(t \to Ws)$ events.

C DNN performance and validation

The ROC curves for all DNNs are shown in Figure 6. The overtraining test for all DNNs are shown in Figure 7. In all categories, the DNN performance on testing dataset agrees well with the training dataset. No overtraining is spotted.

D Fit results including τ lepton categories

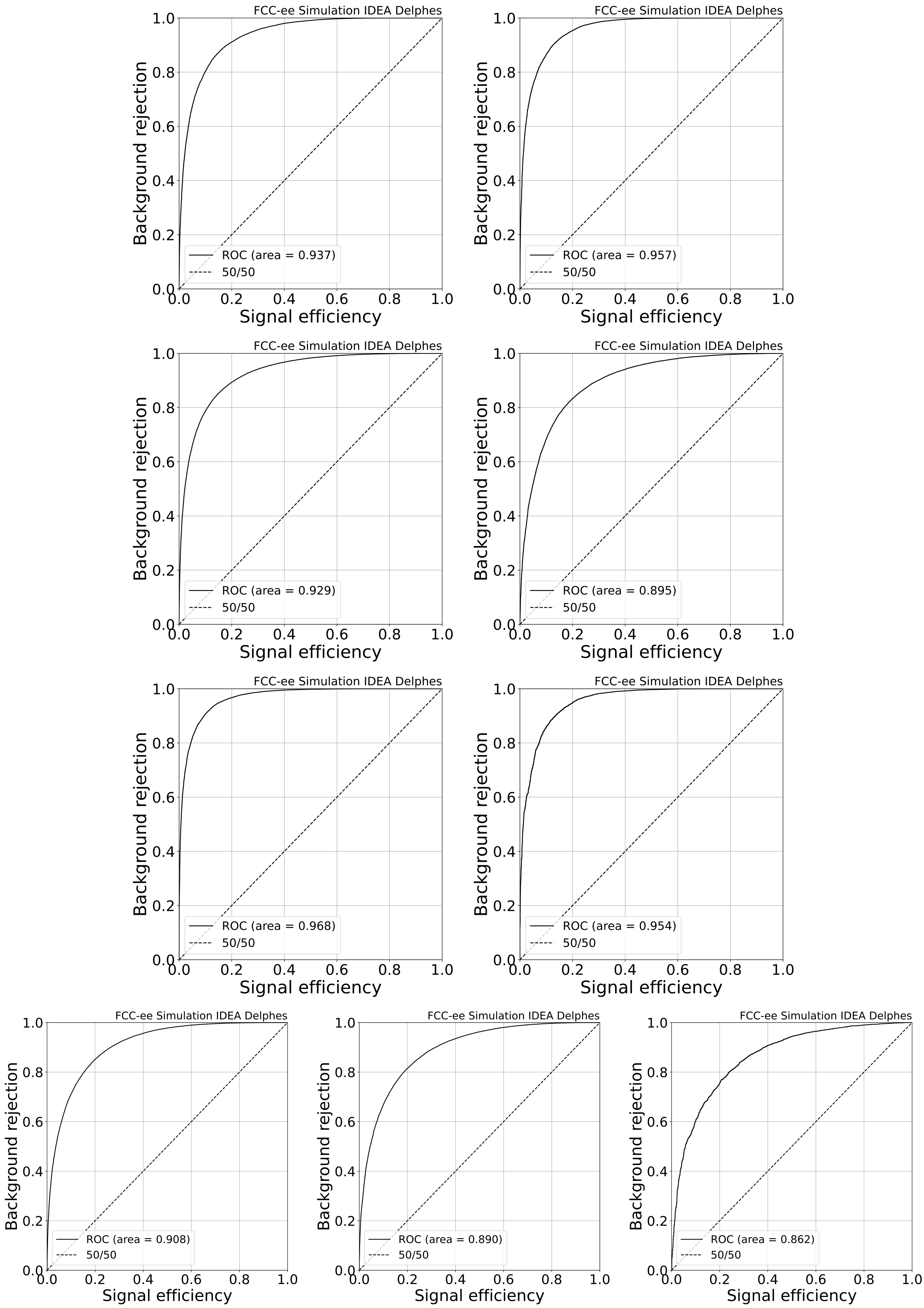

Figure 6: DNN ROC curves, in reading order, in dilep_0tau, dilep_1tau, semilep_0tau_ud, semilep_0tau_cs, semilep_1tau_ud, semilep_1tau_cs, dihad_ud_only, dihad_udcs, and dihad_cs_only categories.

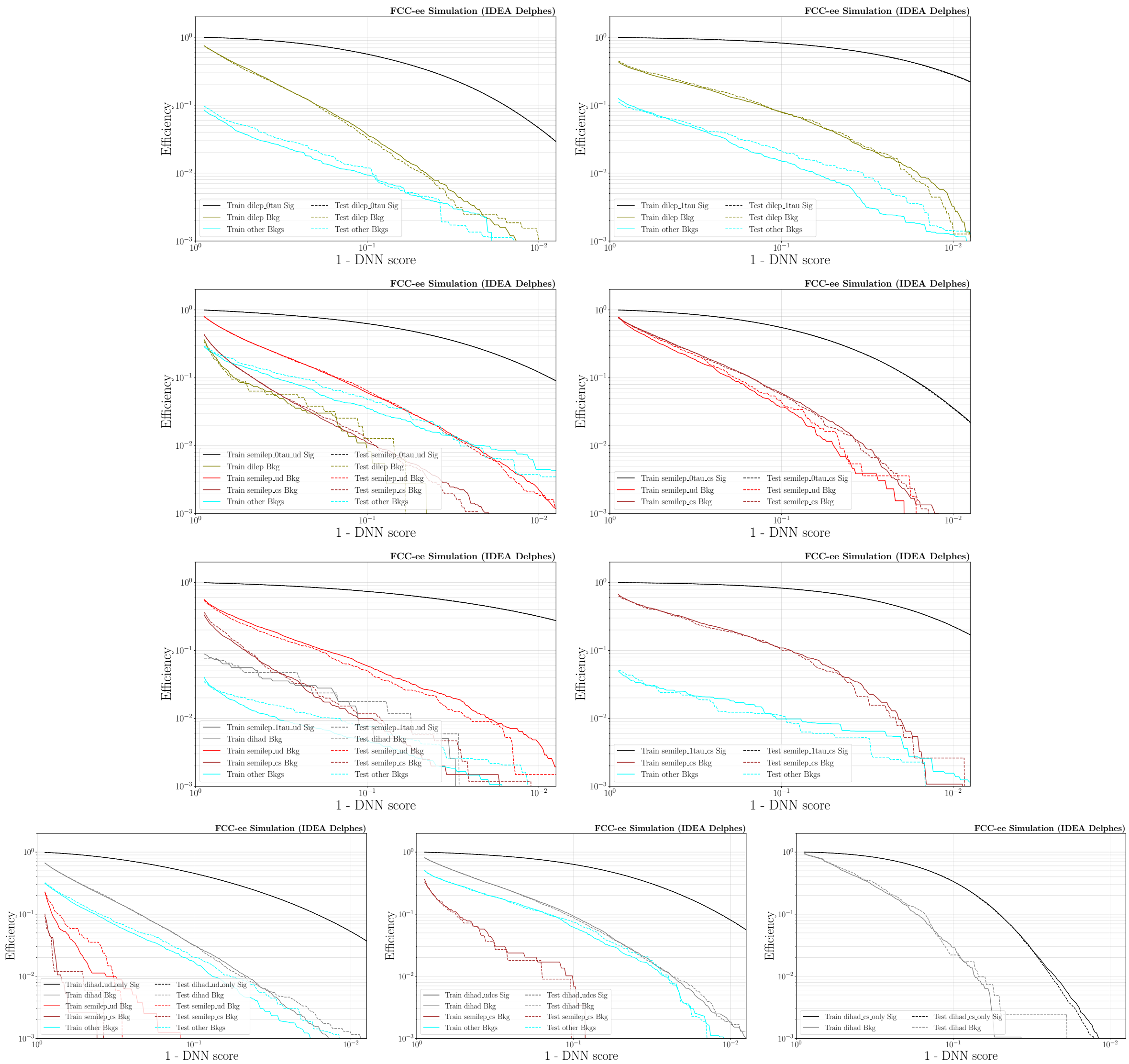

Figure 7: DNN overtraining tests, in reading order, in dilep_0tau, dilep_1tau, semilep_0tau_ud, semilep_0tau_cs, semilep_1tau_ud, semilep_1tau_cs, dihad_ud_only, dihad_udcs, and dihad_cs_only categories.

Fit config	bkg ±1%
category	
dilep_0tau	11.8%
dilep_0tau	18.2%
semilep_0tau_ud	9.7%
semilep_0tau_cs	17.7%
semilep_1tau_ud	19.8%
semilep_1tau_cs	37.8%
dihad_ud_only	18.6%
dihad_udcs	24.1%
dihad_cs_only	76.2%
combined	5.6%

Table 6: Relative uncertainty on $\mathcal{B}(t \to Ws)$ measurement combining all categories. Nominal scenario for background uncertainty is considered: all backgrounds are constrained to 1% variation from their nominal yields.

References

[1] R. L. Workman et al. "Review of Particle Physics". In: *PTEP* 2022 (2022), p. 083C01. DOI: 10.1093/ptep/ptac097.

[2] Y. Aoki et al. "FLAG Review 2021". In: *Eur. Phys. J. C* 82.10 (2022), p. 869. DOI: 10.1140/epjc/s10052-022-10536-1. arXiv: 2111.09849 [hep-lat].

[3] W. Kilian, T. Ohl, and J. Reuter. "WHIZARD: Simulating Multi-Particle Processes at LHC and ILC". In: *Eur. Phys. J. C* 71 (2011), p. 1742. DOI: 10.1140/epjc/s10052-011-1742-y. arXiv: 0708.4233 [hep-ph].

[4] M. Moretti, T. Ohl, and J. Reuter. "O'Mega: An Optimizing matrix element generator". In: (Feb. 2001). Ed. by T. Behnke et al., pp. 1981–2009. arXiv: hep-ph/0102195.

[5] T. Sjostrand, S. Mrenna, and P. Z. Skands. "PYTHIA 6.4 Physics and Manual". In: *JHEP* 05 (2006), p. 026. DOI: 10.1088/1126-6708/2006/05/026. arXiv: hep-ph/0603175.

[6] C. Bierlich et al. "A comprehensive guide to the physics and usage of PYTHIA 8.3". In: (Mar. 2022). DOI: 10.21468/SciPostPhysCodeb.8. arXiv: 2203.11601 [hep-ph].

[7] M Antonello. "IDEA: A detector concept for future leptonic colliders". In: *Nuovo Cimento C* 43.2-3 (2020), p. 27. DOI: 10.1393/ncc/i2020-20027-2. URL: https://cds.cern.ch/record/2770999.

[8] J. de Favereau et al. "DELPHES 3, A modular framework for fast simulation of a generic collider experiment". In: *JHEP* 02 (2014), p. 057. DOI: 10.1007/JHEP02(2014)057. arXiv: 1307.6346 [hep-ex].

[9] M. Cacciari, G. P. Salam, and G. Soyez. "FastJet User Manual". In: *Eur. Phys. J. C* 72 (2012), p. 1896. DOI: 10.1140/epjc/s10052-012-1896-2. arXiv: 1111.6097 [hep-ph].

[10] Franco Bedeschi, Loukas Gouskos, and Michele Selvaggi. "Jet flavour tagging for future colliders with fast simulation". In: *The European Physical Journal C* 82.7 (July 2022). ISSN: 1434-6052. DOI: 10.1140/epjc/s10052-022-10609-1. URL: http://dx.doi.org/10.1140/epjc/s10052-022-10609-1.

[11] Huilin Qu and Loukas Gouskos. “Jet tagging via particle clouds”. In: *Physical Review D* 101.5 (Mar. 2020). ISSN: 2470-0029. DOI: 10.1103/physrevd.101.056019. URL: http://dx.doi.org/10.1103/PhysRevD.101.056019.

[12] A. Hayrapetyan et al. “The CMS Statistical Analysis and Combination Tool: COMBINE”. In: *Submitted to Computing and Software for Big Science* (Apr. 2024). arXiv: 2404.06614 [physics.data-an].